

Estimation of floor response spectra induced by artificial and real earthquake ground motions

Wuchuan Pu* and Xi Xu^a

School of Civil Engineering and Architecture, Wuhan University of Technology,
Luoshi Road 122, Wuhan, 430070 China

(Received June 4, 2018, Revised April 2, 2019, Accepted April 9, 2019)

Abstract. A method for estimating the floor response spectra (FRS) of elastic structures under earthquake excitations is proposed. The method is established based on a previously proposed direct estimation method for single degree of freedom systems, which generally overestimates the FRS of a structure, particularly in the resonance period range. A modification factor is introduced to modify the original method; the modification factor is expressed as a function of the period ratio and is determined through regression analysis on time history analysis results. Both real and artificial ground motions are considered in the analysis, and it is found that the modification factors obtained from the real and artificial ground motions are significantly different. This suggests that the effect of ground motion should be considered in the estimation of FRS. The modified FRS estimation method is further applied to a 10-story building structure, and it is verified that the proposed method can lead to a good estimation of FRS of multi-story buildings.

Keywords: floor response spectra; modal superposition; nonstructural component; artificial ground motion; higher mode

1. Introduction

A building structural system generally consists of the main structure and nonstructural components mounted on the main structure. In seismic design, attention has mostly been paid to the safety of the main structure. The lessons gained from recent major earthquakes have shown that even the number of casualties can be effectively reduced while the economic loss due to damage to nonstructural components or equipment may be very significant. For instance, 2010 Chile earthquake caused widespread nonstructural damage in all types of buildings, while very limited structural damage was observed (Miranda *et al.* 2012; Saatcioglu *et al.* 2013); 2011 Christchurch earthquake also caused widespread nonstructural damage which was more severe than structural damage (Baird *et al.* 2014). For commercial buildings, it has been reported that the cost of nonstructural components and equipment may account for 75–85% of the total construction cost (FEMA 2012). Under earthquake action, building structures still face great risk of economic loss. In order to identify possible economic losses of nonstructural components in the design stage, it is necessary to quantitatively evaluate the response of these components.

Nonstructural components cover a wide range of architectural components, attached electromechanical equipment, and interior furniture etc. Nonstructural components can be divided into acceleration sensitive type,

displacement sensitive type, and the combined type. Acceleration sensitive nonstructural components are directly subjected to the floor acceleration, and the dynamic response depends on both the floor acceleration excitation and the dynamic property of nonstructural component. Floor response spectra (FRS) are commonly employed for estimating the performance or performing seismic design of this type of nonstructural components. FRS can be derived through either a time history analysis or the direct estimation method. Time history analysis is used for very important structural systems, e.g., nuclear plants, for which relatively accurate estimation is required. The direct estimation method is less accurate but more efficient, and it can be used for most common building structures. The direct estimation method has been the focus of researches associated with the FRS of building structures.

Floor response spectra have attracted research attention since a few decades ago. Mayes *et al.* (1983) developed a direct generation method for FRS by combining a stochastic approach with the modal superposition method. Yasui *et al.* (1993) proposed a direct generation method for FRS of an elastic structure. The acceleration response of a nonstructural component is derived theoretically, and the maximum acceleration response of the nonstructural component is approximated as a combination of the maximum acceleration of the main structure and the nonstructural component directly subjected to the input ground motion. Ghosh (2000) presented a scheme for deriving FRS by frequency response function which was calculated numerically. Medina *et al.* (2006) investigated the FRS of light components mounted on regular moment resisting frame structures, through numerical simulations conducted with regular frame structures subjected to a set of

*Corresponding author, Associate Professor
E-mail: puwuchuan@whut.edu.cn

^a M.Sc. Student

40 seismic ground motions. They pointed out that FRS is significantly affected by the modal periods and the strength of the main structure, as well as the location of nonstructural components in the structure and the damping ratio of the component. Shoostari *et al.* (2010) investigated the FRS of concrete frame and frame-shear wall buildings of Canada. Pozzi and Der Kiureghian (2015) proposed a complete quadratic combination (CQC) type rule for computing the peak floor acceleration based on the design spectrum.

The effect of nonlinear behavior of main structure has been extensively studied in recent works. Singh and Chang (1996) pointed out that the FRS of yielding structures can be higher in the high frequency range than the corresponding elastic response spectra, and this is due to the phenomenon of internal resonance encountered in nonlinear vibration. Politopoulos and Feau (2007) investigated the characteristics of FRS of SDOF nonlinear structure and proposed an estimation method. Sankaranarayanan and Medina (2007) investigated the acceleration amplification factor for nonstructural components mounted on inelastic multi-story frame structures. Oropeza *et al.* (2010) also investigated the floor response spectra of nonlinear structures that were simulated by different types of hysteretic models, including an elasto-plastic model, γ -model, modified Takeda model, and Q model. The resonance factor and acceleration amplification were numerically investigated. Sullivan *et al.* (2013) accounted for the period and inelasticity of main structure, and proposed a series of empirical equations for predicting floor response spectra. Vukobratovic and Fajfar (2015, 2016) proposed a method for the direct determination of FRS with the inelastic behavior of the main structure in consideration, for single degree of freedom (SDOF) and multiple degrees of freedom (MDOF) structure, respectively. An extensive numerical study was performed on SDOF structures to clarify the effect of input ground motion, ductility, hysteretic behavior, and the period of the main structure, as well as the damping ratio of the nonstructural component. Based on the formula proposed by Yasui *et al.* (1993), a modification factor was proposed by considering these effects. Flores *et al.* (2015) investigated the floor response spectra, with focus on the modeling approaches of inelastic steel moment frame structures. Pan *et al.* (2017) proposed a modal pushover method to estimate FRS of multi-story building structures. Kothari *et al.* (2017) carried out experimental study on nonlinear concrete structure to examine FRS.

As a common approach, the floor response spectra are generated based on the SDOF structure, and the FRS of multi-story buildings can be obtained using the modal combination method, such as the square root of the sum of squares (SRSS) or CQC method. The direct prediction method developed by Yasui *et al.* (1993) has established a theoretical basis for predicting FRS, and it is easy to use in practice. However, this method significantly overestimates FRS at the resonant period range. Recently, this method has been expanded to inelastic structures; the results of these investigations have shown that FRS of inelastic structures is smaller than that derived from elastic structures

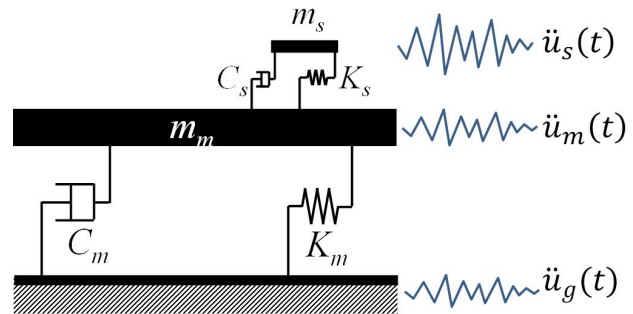


Fig. 1 Analytical model

(Vukobratovic and Fajfar 2015, 2016). The FRS of elastic structures seems more critical for nonstructural components. Moreover, seismic design is usually based on design spectra regulated by seismic codes, and time history analysis is performed by subjecting a structural system to artificial ground motions generated from design spectra. The difference in the properties of ground motions may cause difference in floor acceleration responses, and may further lead to large difference in responses of nonstructural components. However, there are no studies that clarify the difference between the FRS of artificial ground motions and those of real ground motions. With an aim to address these problems, this study aims to propose a modified FRS estimation method based on the original method of Yasui *et al.* (1993), and the characteristics of ground motion (artificial or real ground motion) will be investigated and taken into account in the estimation method. The FRS of multi-story building structures is estimated based on the proposed method, and the effect of the damping model and higher mode effects will be discussed.

2. Original estimation method

The floor acceleration response is derived using the system shown in Fig. 1. The structural system consists of the main structure and the nonstructural component, both of which are simulated as SDOF systems. The mass, stiffness, and damping ratio of the main structure are denoted by m_m , K_m , and ζ_m , respectively; correspondingly, m_s , K_s , and ζ_s denote the mass, stiffness, and damping ratio of the nonstructural component. In the analysis, the mass of the nonstructural component is far smaller than the mass of the main structure, so that the response of the main structure will not be affected by the nonstructural component.

By referring to the work of Yasui *et al.* (1993), when a structural system is subjected to the ground motion $\ddot{u}_g(t)$, the floor response spectra can be estimated using Eq. (1). In Eq. (1), S denotes the acceleration spectra of the input ground motion. From Eq. (1), it is known that FRS is affected by the frequency ratio (ω_s/ω_m), the damping ratio, and the spectral values of both the main structure and the nonstructural component. In an elastic MDOF structural system, considering the contribution of multi-vibration modes, the floor response spectra of floor level j can be expressed as Eq. (2). In Eq. (2), β_i^j is the value of the i -th

$$FRS = \frac{1}{\sqrt{\left(1 - \left(\frac{\omega_s}{\omega_m}\right)^2\right)^2 + 4(\zeta_s + \zeta_m)^2 \left(\frac{\omega_s}{\omega_m}\right)^2}} \sqrt{\left(\left(\frac{\omega_s}{\omega_m}\right)^2 S(\omega_m, \zeta_m)\right)^2 + S(\omega_s, \zeta_s)^2} \quad (1)$$

$$FRS^j = \sqrt{\sum_{i=1}^n (\beta_i^j FRS_i)^2} \quad (2)$$

$$FRS_i = \frac{1}{\sqrt{\left(1 - \left(\frac{\omega_s}{\omega_{m,i}}\right)^2\right)^2 + 4(\zeta_s + \zeta_{m,i})^2 \left(\frac{\omega_s}{\omega_{m,i}}\right)^2}} \sqrt{\left(\left(\frac{\omega_s}{\omega_{m,i}}\right)^2 S(\omega_{m,i}, \zeta_{m,i})\right)^2 + S(\omega_s, \zeta_s)^2} \quad (3)$$

mode shape vector, on level j , and FRS_i denotes the floor response spectra derived from the i -th component of generalized modal coordinate of floor acceleration, as given by Eq. (3). In Eq. (3), those parameters for the i -th mode are all denoted by a subscript i .

3. Modification of direct estimation method

3.1 Modification procedure

Eq. (1) was obtained from a theoretical derivation under specific assumptions. For estimating the FRS more accurately, the method should be improved. For the purpose of modifying the method, a modification factor α is introduced, and Eq. (4) is proposed for estimating the FRS.

$$FRS = \frac{FRS_{ORG}}{\alpha} \quad (4)$$

In Eq. (4), FRS_{ORG} is the FRS estimated by Eq. (1). The modification factor α can be identified by comparing the acceleration responses of the nonstructural component obtained from time history analysis (FRS_{THA}) and those estimated by Eq. (1) (FRS_{ORG}), as given by Eq. (5).

$$\alpha = \frac{FRS_{ORG}}{FRS_{THA}} \quad (5)$$

In the following, a time history analysis is performed by subjecting SDOF structures to real earthquake records and artificial ground motions. Both the period of the main structure and the period of the nonstructural component are assigned between 0.1 and 4.0 s, and an interval of 0.1 s is considered; therefore, 40 periods are considered. The damping ratios for the main structure and the nonstructural component are set to be 0.05 and 0.03, respectively. FRS is computed by inputting the ground motion to each system with a specific period, and FRS is also estimated using Eq. (1) based on the acceleration spectra of ground motions. The modification factors are investigated in the following.

3.2 Modification factor for real ground motions

In order to account for the effect of soil condition, 4 sets

of non-pulse type ground motions recorded on soil type A, B, C and D (based on the USGS category), respectively, are selected from earthquake events with a magnitude between 5.5 and 7.0. Tables 1-4 give the information on each set of ground motions. The duration listed in tables is the interval of time between 5% and 95% of the total Arias intensity. Fig. 2 shows the acceleration response spectra of each ground motion as well as their average in each soil type, in which the peak values of all acceleration time history are scaled to 0.2g. The earthquake records are all obtained from the PEER strong ground motion database.

The modification factor is estimated using Eq. (5). Figs. 3-4 plotted the modification factors against the period ratio of T_m/T_s for soil type A and type D, respectively. Six subfigures are shown for selected different periods T_m . In each subfigure, the modification factors obtained from individual ground motion are shown by gray lines, and their averages are presented by red lines. The modification factor follows a bell-shaped distribution, and the ratio reaches its maximum at $T_m/T_s=1$, and the maximums are larger than 1, which suggests overestimation of FRS obtained using Eq. (1). These observations are common for different periods T_m . It is also observed that there exists a certain discrepancy among the maximum values of the modification factors derived from different ground motions.

According to the observations, it is considered beneficial to simulate the distribution of modification factors by a uniform shape function. Based on this concept, the modification factor is derived using a two-step procedure: the distribution of α is normalized by its maximum, and the normalized distribution shape is simulated as a function of T_m/T_s through a regression analysis, namely, $\alpha_1(T_m/T_s)$; the maximum value is then investigated by considering the possible effect of T_m and the effect of ground motions, and the maximum value is denoted by α_2 . Combining the results of the two steps, the modification factor can be expressed as Eq. (6).

$$\alpha = \alpha_1(T_m/T_s) \cdot \alpha_2 \quad (6)$$

For type A ground motions, Fig. 5(a) shows the distribution of α normalized by their maximums, namely, α_1 . Based on the numerical results, the empirical formula in Eq. (7) is proposed.

Table 1 Ground motions recorded on soil type A

No.	Earthquake(Year)	Mag.	Station	Comp.	PGA (g)	Duration (s)
1	Coyote Lake(1979)	5.74	Gilroy Array #1	N320	0.12	5.78
2	Whittier Narrows-01(1987)	5.99	Pasadena-CIT Kresge Lab	EW	0.11	3.46
3	Parkfird-02_CA(2004)	6.00	Parkfield-Turkey Flat #1	EW	0.25	8.76
4	Parkfird-02_CA(2004)	6.00	Parkfield-Turkey Flat #1	NS	0.20	8.26
5	Morgan Hill(1984)	6.19	Gilroy Array #1	N320	0.10	8.93
6	Tottori_Japan(2000)	6.61	OKYH07	NS	0.18	18.24
7	Tottori_Japan(2000)	6.61	OKYH07	EW	0.13	19.56
8	Tottori_Japan(2000)	6.61	SMNH10	NS	0.16	12.84
9	Tottori_Japan(2000)	6.61	SMNH10	EW	0.23	9.20
10	Niigata_Japan(2004)	6.63	FKSH07	NS	0.14	15.84
11	Niigata_Japan(2004)	6.63	FKSH07	EW	0.10	16.70
12	Northridge-01(1994)	6.69	LA-Wonderland Ave	N95	0.10	8.72
13	Northridge-01(1994)	6.69	LA-Wonderland Ave	N185	0.16	6.67
14	Northridge-01(1994)	6.69	Vasquez Rocks Park	NS	0.15	8.27
15	Northridge-01(1994)	6.69	Vasquez Rocks Park	EW	0.14	7.34
16	Kobe_Japan(1995)	6.90	Kobe University	NS	0.28	7.04
17	Kobe_Japan(1995)	6.90	Kobe University	EW	0.31	6.20
18	Loma Prieta(1989)	6.93	Gilroy Array #1	NS	0.43	6.55
19	Loma Prieta(1989)	6.93	Gilroy Array #1	EW	0.48	3.70
20	Loma Prieta(1989)	6.93	So. San Francisco_Sierra Pt.	N205	0.11	9.64

Table 2 Ground motions recorded on soil type B

No.	Earthquake(Year)	Mag.	Station	Comp.	PGA (g)	Duration (s)
1	Helena_Montana-01(1935)	6.00	Carroll College	NS	0.16	2.41
2	Helena_Montana-01(1935)	6.00	Carroll College	EW	0.16	2.54
3	Parkfield(1966)	6.19	Temblor pre-1969	N205	0.36	4.45
4	Parkfield(1966)	6.19	Temblor pre-1969	N295	0.27	5.46
5	San Fernando(1971)	6.61	Castaic - Old Ridge Route	N21	0.32	15.47
6	San Fernando(1971)	6.61	Castaic - Old Ridge Route	N291	0.28	16.76
7	San Fernando(1971)	6.61	Lake Hughes #9	N21	0.17	9.33
8	San Fernando(1971)	6.61	Lake Hughes #9	N291	0.14	11.84
9	San Fernando(1971)	6.61	Pearblossom Pump	NS	0.10	13.74
10	San Fernando(1971)	6.61	Pearblossom Pump	EW	0.14	13.65
11	San Fernando(1971)	6.61	Fairmont Dam	N326	0.11	12.98
12	Norcia Italy(1979)	5.90	Cascia	EW	0.21	5.20
13	Norcia Italy(1979)	5.90	Cascia	NS	0.15	5.69
14	Mammoth Lakes-01(1980)	6.06	Long Valley Dam	NS	0.43	10.91
15	Mammoth Lakes-01(1980)	6.06	Long Valley Dam	EW	0.27	10.85
16	Mammoth Lakes-02(1980)	5.69	Long Valley Dam	NS	0.19	8.72
17	Victoria Mexico(1980)	6.33	Cerro Prieto	N45	0.64	8.25
18	Victoria Mexico(1980)	6.33	Cerro Prieto	N315	0.63	7.53
19	Imperial Valley-06(1979)	6.53	Cerro Prieto	N147	0.17	30.04
20	Imperial Valley-06(1979)	6.53	Cerro Prieto	N237	0.16	36.41

Table 3 Ground motions recorded on soil type C

No.	Earthquake(Year)	Mag.	Station	Comp.	PGA (g)	Duration (s)
1	Imperial Valley-02(1940)	6.95	EI Centro Array #9	NS	0.28	24.19
2	Imperial Valley-02(1940)	6.95	EI Centro Array #9	EW	0.21	24.15
3	Northern Calif-01(1941)	6.40	Ferndale City Hall	N225	0.11	13.03
4	Northern Calif-01(1941)	6.40	Ferndale City Hall	N315	0.12	15.48
5	Northwest Calif-03(1951)	5.80	Ferndale City Hall	N224	0.11	14.45
6	Imperial Valley-06(1979)	6.53	Bonds Corner	N140	0.60	9.65
7	Parkfield(1966)	6.19	Cholame - Shandon Array #5	N85	0.44	6.51
8	Parkfield(1966)	6.19	Cholame - Shandon Array #5	N355	0.37	7.48
9	Parkfield(1966)	6.19	Cholame - Shandon Array #8	N50	0.25	13.13
10	Parkfield(1966)	6.19	Cholame - Shandon Array #8	N320	0.27	10.77
11	Imperial Valley-06(1979)	6.53	Bonds Corner	N230	0.78	9.75
12	Managua Nicaragua-01(1972)	6.24	Managua_ ESSO	EW	0.37	10.63
13	Managua Nicaragua-01(1972)	6.24	Managua_ ESSO	NS	0.33	8.23
14	San Fernando(1971)	6.61	Gormon - Oso Pump Plant	EW	0.10	7.16
15	San Fernando(1971)	6.61	LA - Hollywood Stor FF	EW	0.22	13.15
16	San Fernando(1971)	6.61	LA - Hollywood Stor FF	NS	0.19	13.42
17	Imperial Valley-06(1979)	6.53	Aeropuerto Mexicali	N45	0.31	9.76
18	Imperial Valley-06(1979)	6.53	Aeropuerto Mexicali	N135	0.27	8.71
19	Imperial Valley-06(1979)	6.53	Calexico Fire Station	N225	0.28	11.04
20	Imperial Valley-06(1979)	6.53	Calexico Fire Station	N315	0.20	14.81

Table 4 Ground motions recorded on soil type D

No.	Earthquake(Year)	Mag.	Station	Comp.	PGA (g)	Duration (s)
1	Coalinga-01(1983)	6.36	Parkfield - Cholame 2WA	NS	0.11	16.64
2	Coalinga-01(1983)	6.36	Parkfield - Cholame 2WA	EW	0.11	17.76
3	Coalinga-01(1983)	6.36	Parkfield - Fault Zone 1	NS	0.14	19.60
4	Coalinga-01(1983)	6.36	Parkfield - Fault Zone 1	EW	0.11	30.82
5	Whittier Narrows-01(1987)	5.99	Carson - Water St	NS	0.11	15.13
6	Superstition Hills-01(1987)	6.22	Imperial Valley Wildlife Liquefaction Array	EW	0.13	15.24
7	Superstition Hills-01(1987)	6.22	Imperial Valley Wildlife Liquefaction Array	NS	0.13	15.15
8	Superstition Hills-02(1987)	6.54	Imperial Valley Wildlife Liquefaction Array	EW	0.18	35.81
9	Superstition Hills-02(1987)	6.54	Imperial Valley Wildlife Liquefaction Array	NS	0.21	34.24
10	Loma Prieta(1989)	6.93	APEEL 2 - Redwood City	N43	0.27	8.41
11	Loma Prieta(1989)	6.93	APEEL 2 - Redwood City	N143	0.22	11.79
12	Loma Prieta(1989)	6.93	Foster City - APEEL 1	NS	0.26	23.15
13	Loma Prieta(1989)	6.93	Foster City - APEEL 1	EW	0.28	14.28
14	Loma Prieta(1989)	6.93	Foster City - Menhaden Court	EW	0.11	15.48
15	Loma Prieta(1989)	6.93	Foster City - Menhaden Court	NS	0.12	13.34
16	Loma Prieta(1989)	6.93	Larkspur Ferry Terminal (FF)	EW	0.14	9.09
17	Loma Prieta(1989)	6.93	Treasure Island	NS	0.10	5.79
18	Loma Prieta(1989)	6.93	Treasure Island	EW	0.16	4.46
19	Tottori_ Japan(2000)	6.61	SMN002	NS	0.15	15.56
20	Tottori_ Japan(2000)	6.61	SMN002	EW	0.18	13.98

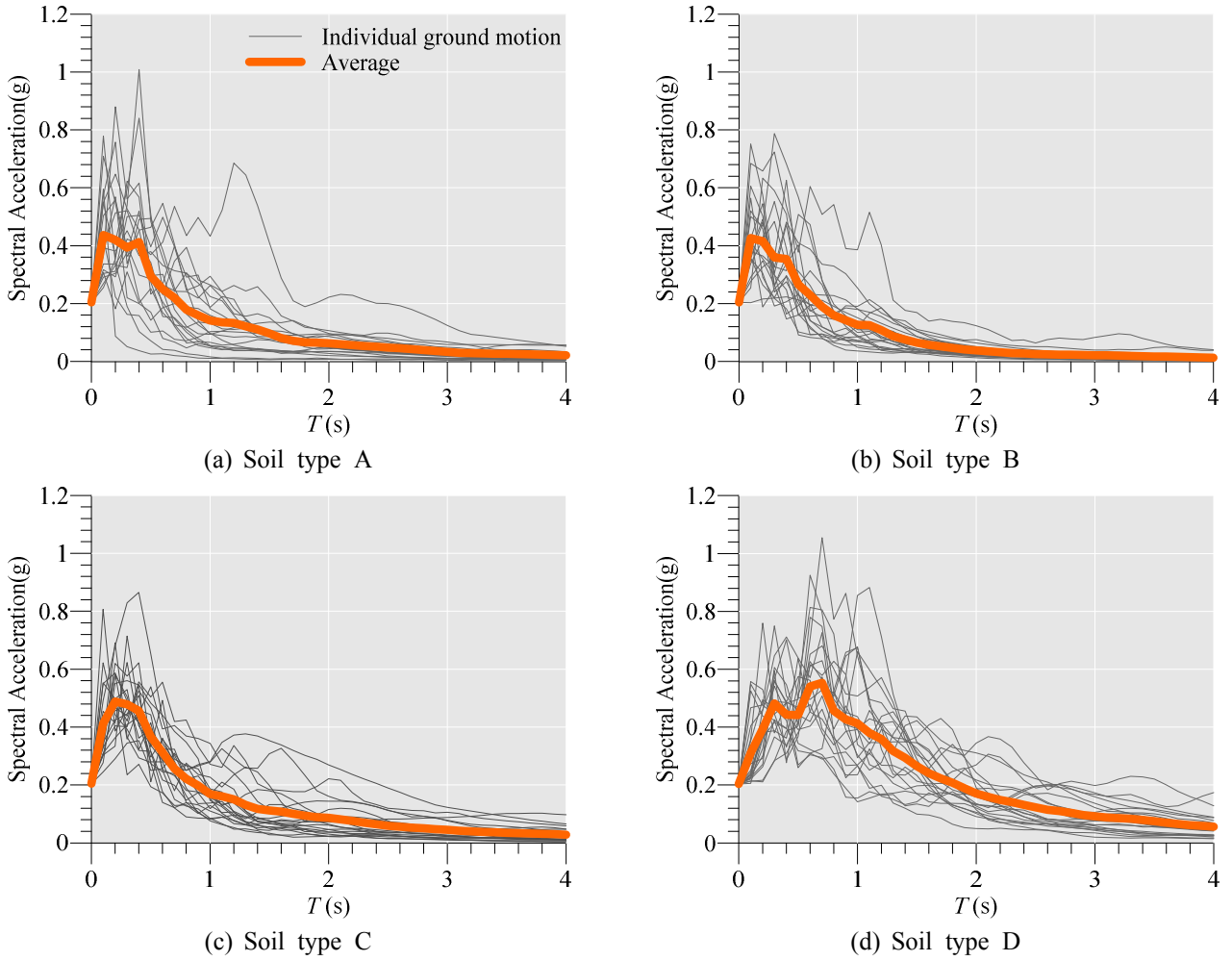


Fig. 2 Acceleration spectra of selected ground motions

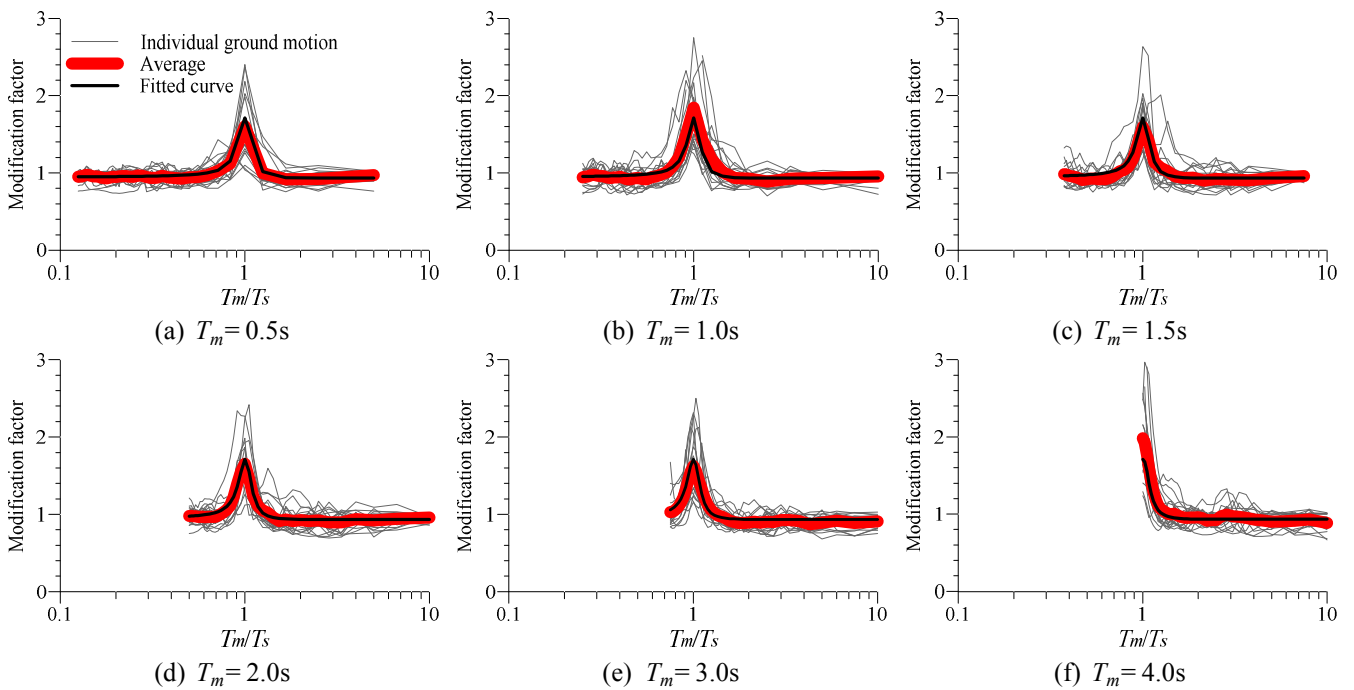


Fig. 3 The ratios between the estimated and computed FRS for soil type A

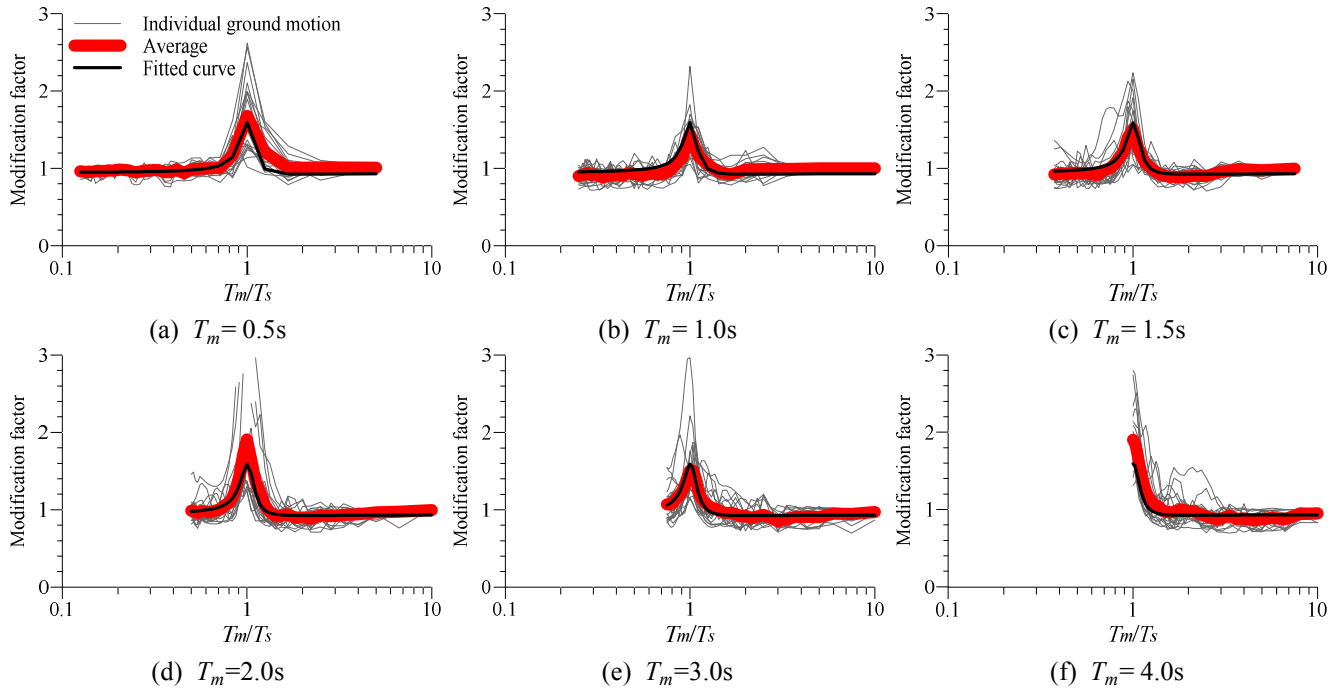


Fig. 4 The ratios between the estimated and computed FRS for soil type D

$$\alpha_1 = \frac{1-c_1\lambda+c_2\lambda^2}{1-c_3\lambda+c_4\lambda^2}, \text{ where } \lambda = \log \frac{T_m}{T_s} \quad (7)$$

The α_1 derived from Eq. (7) is illustrated in Fig. 5(a) by a black line. Fig. 5(b) shows the distribution of the maximum of α denoted by cross symbols. The maximum ratios mostly range between 1.0 and 2.5, and no significant dependency on T_m is observed in the period range considered. Therefore, the average of these maximum values, 1.71, is adopted to represent these maximums. Fig. 6 shows the regression results for type D ground motions. Table 5 gives the regressed values for the coefficients, c_1 , c_2 , c_3 , c_4 and α_2 included in Eq. (6) and Eq. (7). It can be observed that relatively smaller value is obtained for soft soil ground motions. Generally, ground motions recorded on soft sites have relatively longer predominant period and longer duration, compared to the ground motions of stiff sites. These features may cause the difference in the response of nonstructural components, as will be discussed in section 3.4.

In Fig. 3 and Fig. 4, the modification factors computed by using the coefficients of Table 5 are illustrated by black lines for comparison. It is seen that proposed empirical modification factors fits the average of the modification factors very well. The modified FRS can be estimated by substituting Eq. (6) and Eq. (7) into Eq. (4).

3.3 Modification factor for artificial ground motions

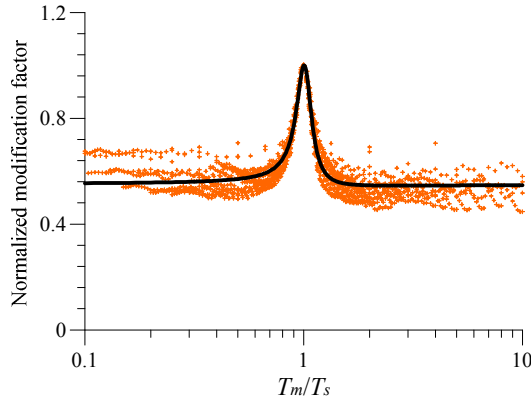
In a similar way, the modification factor for artificial ground motions is investigated. The artificial ground motions can be generated by a time-domain method (e.g. Lihanand and Tseng 1988, Cai and Sheng 1997) or a frequency-domain method. The frequency-domain method based on Fourier transformation is the most typical method

Table 5 Regressed coefficients of Eq. (6) and Eq. (7) for different types of ground motion

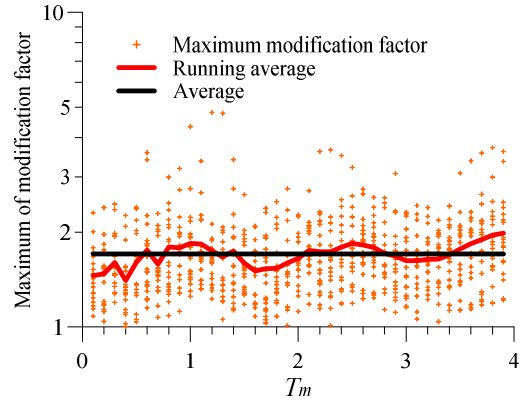
	Type A	Type B	Type C	Type D	Artificial ground motion
c_1	5.7	9.8	12.4	7.7	16.5
c_2	302	202	223	288	509
c_3	6.6	11.8	14.3	8.7	18.6
c_4	549	361	389	488	713
α_2	1.71	1.65	1.63	1.59	1.37

for generating artificial ground motion, and it has been included in many earthquake record processing programs such as SeismoArtif released by Seismosoft (2013). Time-domain methods and frequency-domain methods are different in their calculation algorithm, computation efficiency, etc. A ground motion is characterized by its intensity, duration and frequency components, and these features can be adjusted in generating artificial ground motions through either a time-domain method or a frequency-domain method. Therefore, the frequency-domain method will be adopted without comparison of the effect of artificial ground motion generation algorithm. The design spectrum defined in the Chinese seismic code (2010) is adopted as a target spectrum. A total of 8 ground motions are generated using the program SeismoArtif. The time length of each ground motion is 40 s, the averaged significant duration is about 30 s, and the time step is 0.01s. Fig. 7 shows the target spectrum as well as the spectrum of each ground motion.

Fig. 8(a) shows the normalized modification factor and the fitted curve, and Fig. 8(b) shows the distribution of the maximum modification factors as well as their running average and whole average. Through the same procedure,

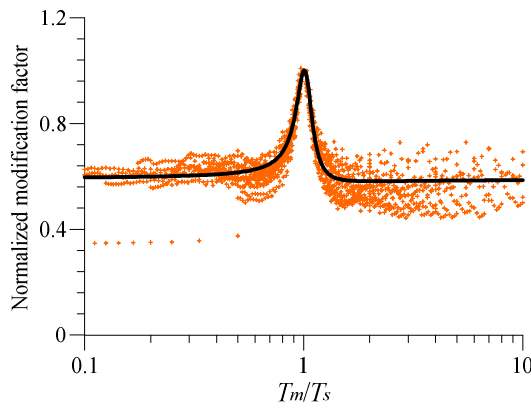


(a) Fitting of the shape function

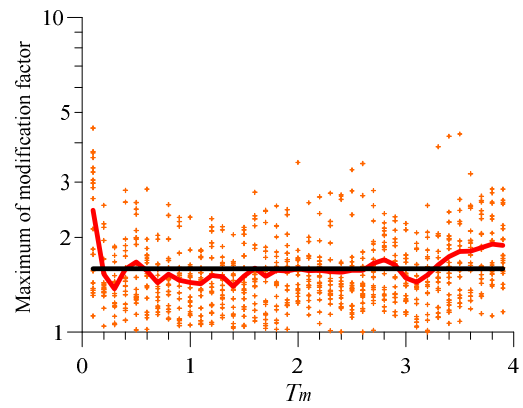


(b) Distribution of maximum modification factor

Fig. 5 Regression of the coefficients of the empirical equation for soil type A



(a) Fitting of the shape function



(b) Distribution of maximum modification factor

Fig. 6 Regression of the coefficients of the empirical equation for soil type D

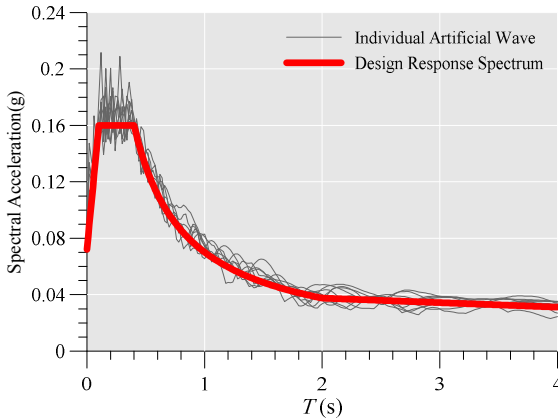


Fig. 7 Acceleration spectra derived from artificial ground motions (5% damping ratio)

3.4 Discussion on the difference between real and artificial ground motions

The above results have shown that the maximum modification factors of artificial ground motions are smaller than those of real ground motions. This means that the original method generally overestimate the FRS less significantly for artificial ground motions, and these results suggest that the real and artificial ground motions should be treated differently when deriving the FRS.

Consider a system with $T_s = T_m$, the following equation can be derived through repeated Duhamel integration (Yasui *et al.* 1993).

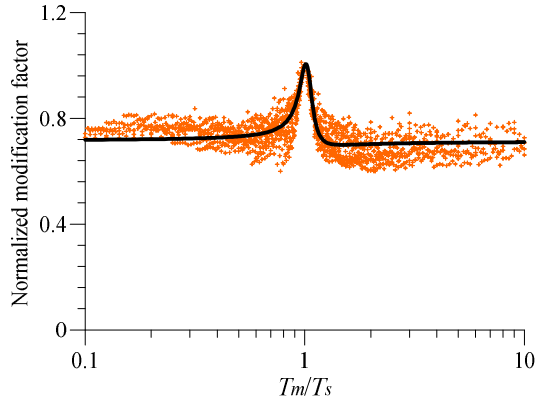
$$2(\zeta_s - \zeta_m)\omega_s \dot{u}_s(t) \approx \ddot{u}_m(t) - \ddot{u}_{s,g}(t) \quad (8)$$

In Eq. (8), $\ddot{u}_m(t)$ and $\ddot{u}_{s,g}(t)$ are the acceleration responses of the main structure and the nonstructural component, respectively, subjected directly to the ground motion, $\dot{u}_s(t)$ is the velocity of nonstructural component. Using $\ddot{u}_s(t)$ to approximate $\omega_s \dot{u}_s(t)$, Eq. (8) can be rewritten as Eq. (9).

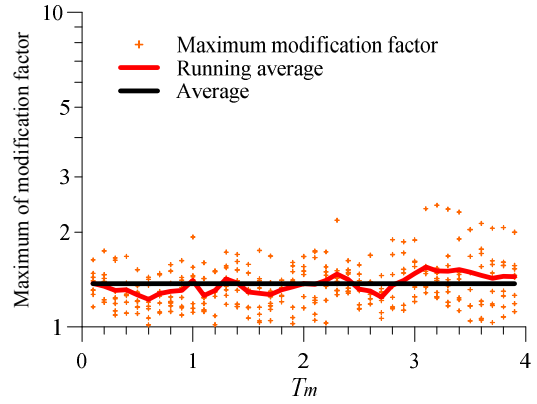
$$2(\zeta_s - \zeta_m)\ddot{u}_s(t) \approx \ddot{u}_m(t) - \ddot{u}_{s,g}(t) \quad (9)$$

Namely, the floor acceleration response $\ddot{u}_s(t)$ can be expressed as the linear summation of $\ddot{u}_m(t)$ and $\ddot{u}_{s,g}(t)$. For estimating the maximum value of $\ddot{u}_s(t)$, the maximums of $\ddot{u}_m(t)$ and $\ddot{u}_{s,g}(t)$, namely, the spectral values $S(\omega_m, \zeta_m)$ and $S(\omega_s, \zeta_s)$ of input ground motion, are combined based on SRSS rule. How the maximums of $\ddot{u}_m(t)$ and $\ddot{u}_{s,g}(t)$ are related to the maximum of $\ddot{u}_s(t)$ affects the accuracy of the estimation of FRS.

Assume $T_s = T_m = 1$ s, $\zeta_s = 0.03$, and $\zeta_m = 0.05$. Fig. 9(a) shows the acceleration time history of ground motion No.1 of Table 1, and Fig. 9(b) shows the time history of $\ddot{u}_m(t)$, $\ddot{u}_{s,g}(t)$ and $\ddot{u}_m(t) - \ddot{u}_{s,g}(t)$. It is known from the computation

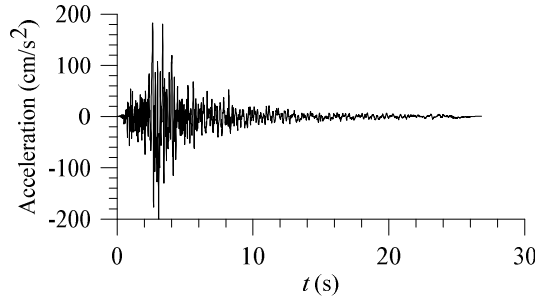


(a) Fitting of the shape function

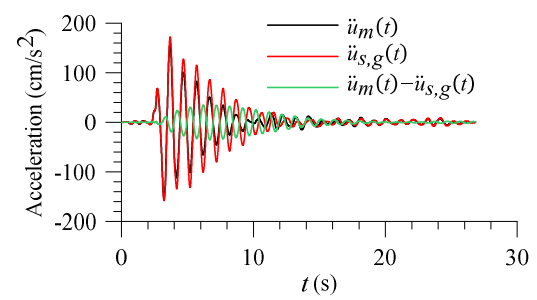


(b) Distribution of maximum modification factor

Fig. 8 Regression of the coefficients of the empirical equation for artificial ground motions

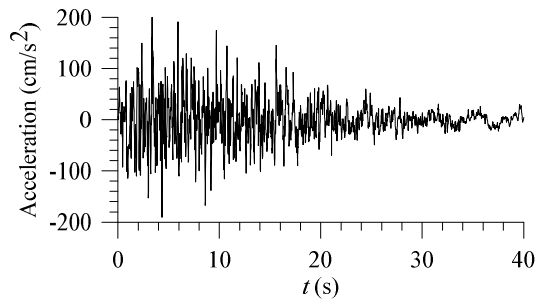


(a) Input ground motion

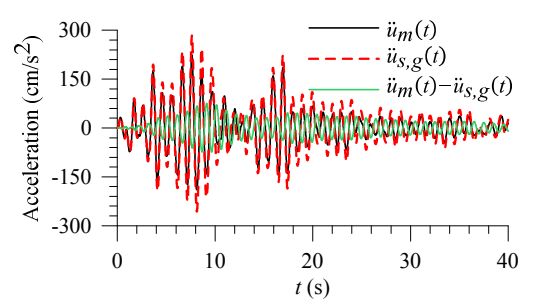


(b) Acceleration responses

Fig. 9 Time history of real ground motion (type A) and responses of structural system



(a) Input ground motion



(b) Acceleration responses

Fig. 10 Time history of artificial ground motion and responses of structural system

results that: $\ddot{u}_m(t)|_{\max} = 156.41 \text{ cm/s}^2$ at $t = 3.680 \text{ s}$; $\ddot{u}_{s,g}(t)|_{\max} = 172.27 \text{ cm/s}^2$ at $t = 3.685 \text{ s}$; $\{\ddot{u}_m(t) - \ddot{u}_{s,g}(t)\}|_{\max} = 35.168 \text{ cm/s}^2$ at $t = 6.690 \text{ s}$. The maximums of $\ddot{u}_m(t)$ and $\ddot{u}_{s,g}(t)$ occur at almost the same time, however, the maximum of $\ddot{u}_m(t) - \ddot{u}_{s,g}(t)$ occurs about 3 seconds later. The absolute value of $\{\ddot{u}_m(t)|_{\max} - \ddot{u}_{s,g}(t)|_{\max}\}$ is only 45 percentage of the value of $\{\ddot{u}_m(t) - \ddot{u}_{s,g}(t)\}|_{\max}$. This means the maximums of $\ddot{u}_m(t)$ and $\ddot{u}_{s,g}(t)$ are very close, and their difference is less correlated to the absolute maximum of $\ddot{u}_m(t) - \ddot{u}_{s,g}(t)$. Corresponding to Fig. 9, Fig. 10 shows the time history of an artificial ground motion and the resulting structural responses. In this case, it is obtained that: $\ddot{u}_m(t)|_{\max} = 224.2 \text{ cm/s}^2$ at $t = 7.63 \text{ s}$; $\ddot{u}_{s,g}(t)|_{\max} = 283.6 \text{ cm/s}^2$ at $t = 7.64 \text{ s}$; $\{\ddot{u}_m(t) - \ddot{u}_{s,g}(t)\}|_{\max} = 75.72 \text{ cm/s}^2$ at $t = 9.14 \text{ s}$. Similarly, the maximums of $\ddot{u}_m(t)$ and $\ddot{u}_{s,g}(t)$

occur almost at the same time, however, the time interval between these maximums and $\{\ddot{u}_m(t) - \ddot{u}_{s,g}(t)\}|_{\max}$ is about 1 second, and the absolute value of $\{\ddot{u}_m(t)|_{\max} - \ddot{u}_{s,g}(t)|_{\max}\}$ is 78 percentage of $\{\ddot{u}_m(t) - \ddot{u}_{s,g}(t)\}|_{\max}$. The difference between the maximums of $\ddot{u}_m(t)$ and $\ddot{u}_{s,g}(t)$ is more correlated to the absolute maximum of $\ddot{u}_m(t) - \ddot{u}_{s,g}(t)$.

In case of artificial ground motions with long durations, the number of cycles and the corresponding duration are greater than that of real ground motions, and this makes that the response of small damping system can be fully excited, and thus the $\{\ddot{u}_m(t) - \ddot{u}_{s,g}(t)\}|_{\max}$ is strongly correlated with $\ddot{u}_m(t)|_{\max}$ and $\ddot{u}_{s,g}(t)|_{\max}$. Therefore, the estimation of FRS based on $\ddot{u}_m(t)|_{\max}$ and $\ddot{u}_{s,g}(t)|_{\max}$ will be more accurate for artificial ground motions.

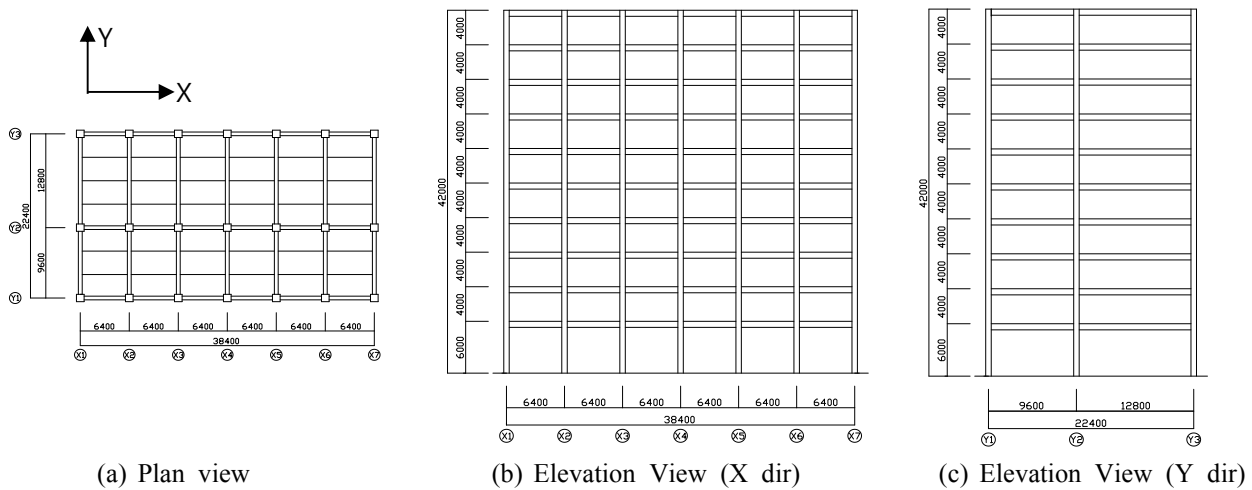


Fig. 11 Plan and elevation of a 10-story building structure (Unit: mm)

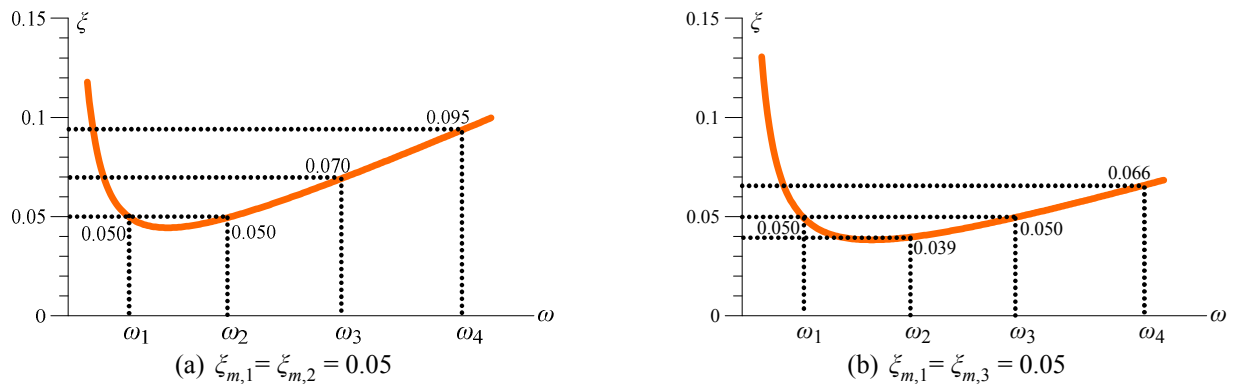


Fig. 12 Damping ratios for the first four modes

4. Estimation of FRS of multi-story building structures

4.1 Structural model

The 10-story benchmark structure defined by JSSI (2003) is adopted to perform a time history analysis. The height of the first story is 6 m, and the height of all other stories is 4 m. There are six spans in the longitudinal (X) direction, and the width of each span is 6.4 m; there are two spans in the transverse (Y) direction, and the span widths are 9.6 m and 12.8 m, respectively. The SN490 steel material is defined for all structural members. A box section and a double tee section are adopted for column and beam members, respectively. The member size is adjusted so that the relationship of $T_1 = 0.05H$ is achieved, where T_1 and H are the fundamental vibration period and the structural height, respectively. The design dead load (D) is 8790 N/m², 7100 N/m², and 5950 N/m² for the top floor, first floor, and remaining floors, respectively. The live load (L) is 600 N/m², 800 N/m², and 800 N/m² for the top floor, first floor, and remaining floors, respectively. These loads are considered in a combination of 1.0 D + 0.5 L.

The three-dimensional model of the structure is created using Midas Gen. Fig. 11 shows the plan and elevation views. The structure is slightly asymmetric in the X-direction, the direction in which seismic excitation is

applied. In the X-direction, the periods of the first four translation modes are 2.02 s, 0.74 s, 0.44 s, and 0.30 s. A rigid floor is assumed, and the acceleration at the mass center of the floor is output as the floor acceleration. The floor acceleration is further input to nonstructural components to derive the acceleration response by using a Matlab-based program. The damping ratio of the nonstructural component is 0.03. There are different ways to define the damping model of multi-story buildings, and the effect of the damping model is investigated as described later.

4.2 Effect of damping models of the main structure

The modal damping and Rayleigh damping, which are widely employed in engineering practice, are adopted for simulating the internal damping effect of the main structure. In case of modal damping, all modes are assigned with a damping ratio of 0.05 (case A). In case of Rayleigh damping, the mass and stiffness proportional coefficients are usually defined by assigning damping ratios for two specific vibration models. In the analysis, two cases are considered: (1) $\zeta_{m,1} = \zeta_{m,2} = 0.05$ (case B); (2) $\zeta_{m,1} = \zeta_{m,3} = 0.05$ (case C), and the damping ratios for the first four modes of these two cases are illustrated in Fig. 12(a) and Fig. 12(b), respectively.

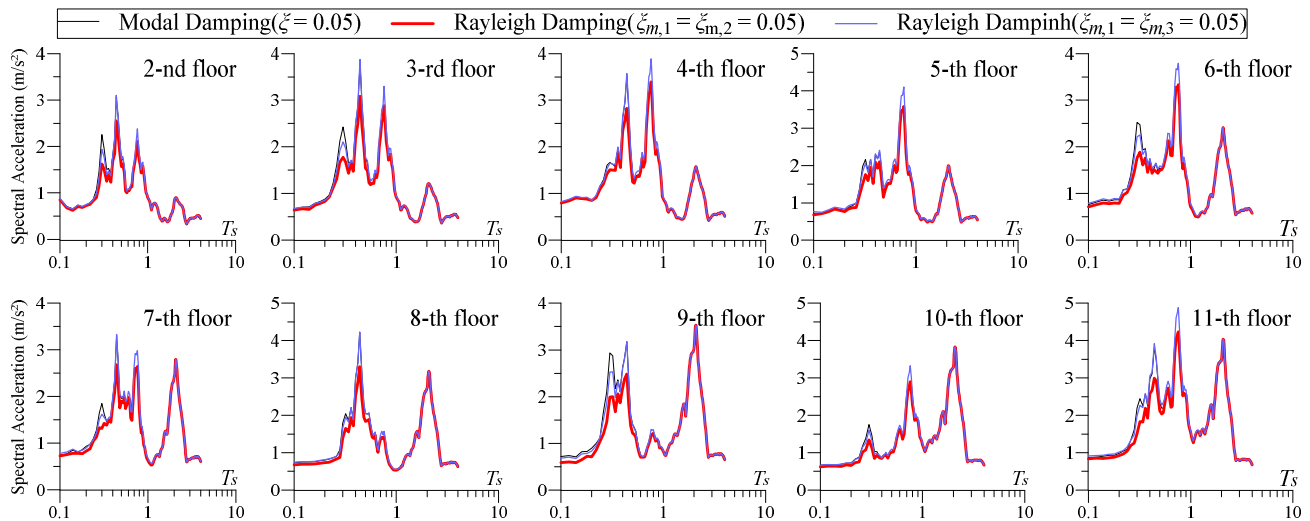


Fig. 13 FRS resulting from different damping models

Fig. 13 shows the FRS derived from the 10-story building with different damping models. The most significant difference induced by different damping models is observed in the short period range, in which the response is mainly excited by higher modes. Due to the different damping ratios of higher modes, the nonstructural components in resonance with higher modes are excited to a different level. This discrepancy is significantly dependent on the story level. For instance, at the 9th floor, the FRS of case B is 31% smaller than that of case A, due to a larger damping ratio of 0.095 of case B compared with the damping ratio of 0.05 of case A. In design practice, attention should be paid to the fact that the FRS of higher modes may be underestimated because of the large damping ratio of higher modes in the Rayleigh damping model.

4.3 Contribution of vibration modes of the main structure to FRS

For elastic MDOF structures, the FRS are estimated by combining the FRS induced by individual vibration modes. SRSS and CQC are typical methods for modal combination. For regular building structures with well-separated modal frequencies subjected to wide-band ground motions, SRSS is considered appropriate for deriving the response. The number of vibration modes that should be taken into account is usually determined by adopting that the sum of their effective mass should exceed a specific percentage of the total mass, e.g., 90%.

It is expected that the acceleration of the nonstructural component with a small damping ratio will be larger than the floor acceleration, as observed in structural acceleration responses, which is usually larger than ground acceleration. This amplification of acceleration may become significant when the nonstructural component is resonant to a vibration mode with a considerable contribution to floor acceleration. In order to verify this effect, the structural modal contribution to the FRS is investigated.

Based on eigenvalue analysis results, the contribution of the first four translation modes of the 10-story building in

the X-direction to the effective mass are 72.9%, 10.7%, 3.5%, and 1.3%. The FRS induced by a normalized modal response is estimated using Eq. (3) and shown in Fig. 14. It should be noted that the contributions of the two torsional modes to effective mass in the X-direction are 8.8% and 1.0%. Even though the effective mass contribution of these two modes looks large, their contribution to floor acceleration is very small; therefore, their contributions to FRS are neglected.

Fig.15 shows the FRS of all levels obtained from each individual ground motion as well as their average. The FRS is estimated using Eq. (2) by considering the first three or the first four translation modes, as shown in Fig. 13 by blue and red lines, respectively. It is observed that the first three modes produce an estimation for most floor levels which is accurate enough, but for some levels (e.g., the 6th and 9th stories) the contribution of the 4th translation mode is very large. The FRS excited by the 4th mode is almost on the same level of the FRS excited by lower modes. Ignoring the effect of 4th mode may cause underestimation of the response of the nonstructural component in resonance with the 4th mode of the main structure. Higher modes that have a small effective mass contribution and can be neglected in the estimation of displacement may lead to significant contribution to acceleration, and therefore, the contribution of higher modes to FRS should be carefully considered in practice.

4.4 Application of the modified FRS method to MDOF structure

In Fig. 15, the FRS derived from the artificial ground motions as well as those estimated by the modified method have already been shown. It can be observed that the modified method can lead to good estimation. It should also be noted that there exists a discrepancy among individual ground motions. For comparison, Figs. 16-18 compare the FRS obtained from real and artificial ground motions, respectively. Fig. 16 is obtained from the No. 20 ground motion in Table 1; Fig. 17 is obtained from the No. 18 ground motion in Table 4; Fig. 18 is obtained from one

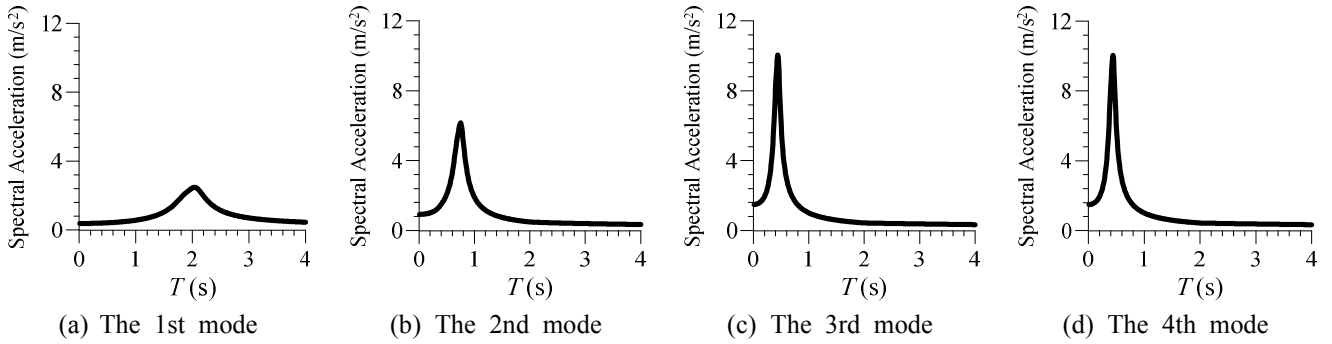


Fig. 14 The modal contribution of the first four vibration modes

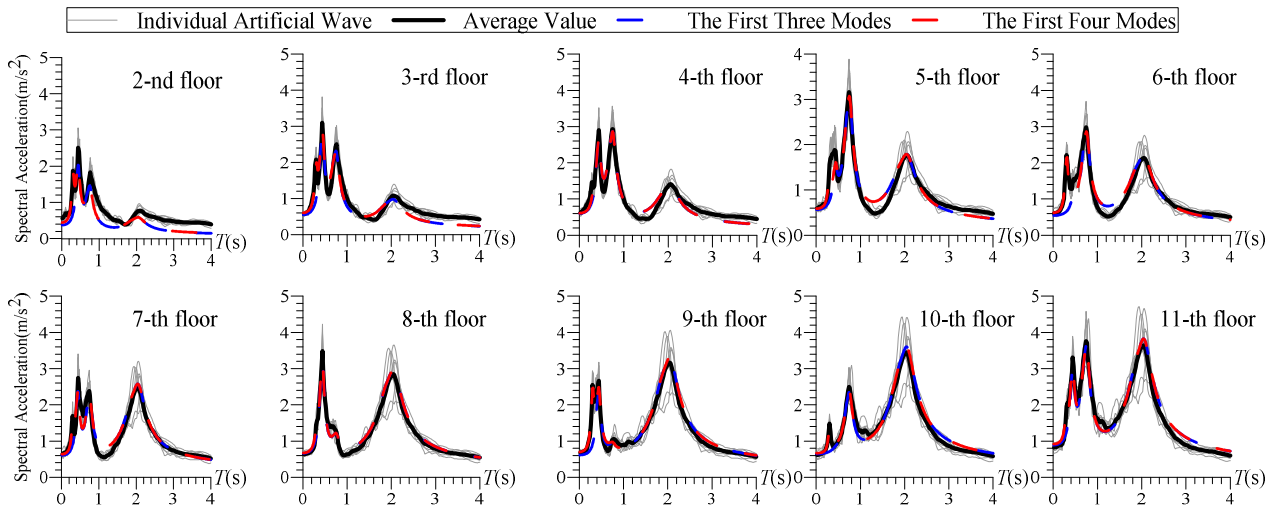


Fig. 15 Comparison of FRS

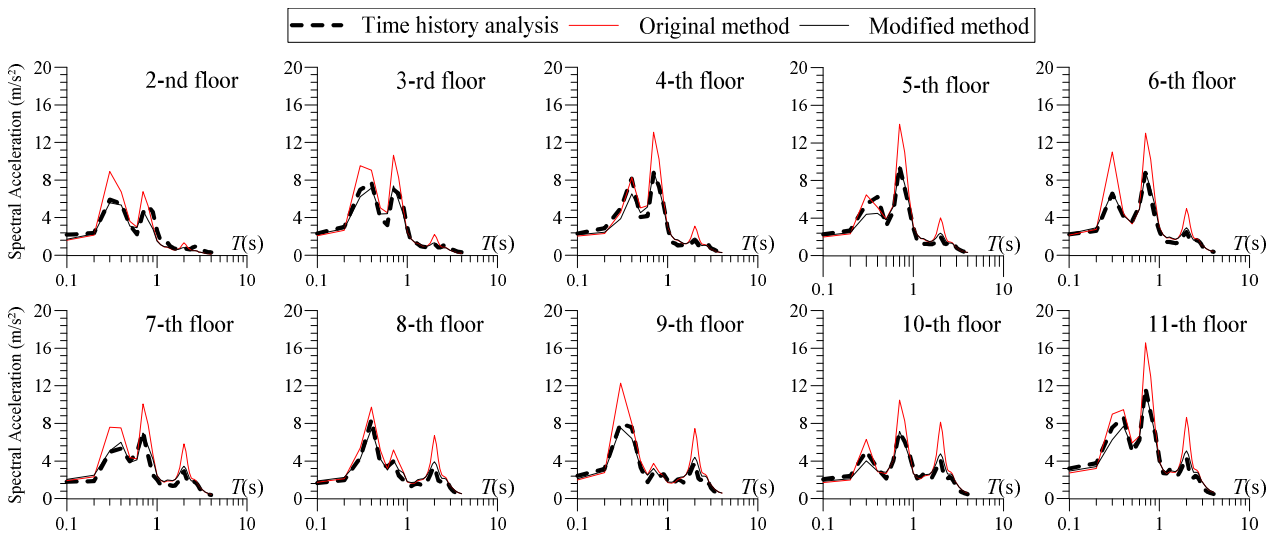


Fig. 16 Comparison of FRS derived from No. 20 ground motion in Table 1 (soil type A)

artificial ground motion. In each figure, the FRS obtained from time history analysis, the FRS estimated by the original method, and the modified method are illustrated. It is seen that the original method overestimated the FRS at all resonant period ranges, and the proposed modified method leads to a more accurate estimation of FRS. By using different modification factors, the modified method is applicable for both artificial and real ground motions.

5. Conclusions

Based on the FRS derived by Yasui *et al.* (1993), a procedure for modifying the FRS estimation formula is proposed. The proposed method is applied to SDOF and MDOF structures, and its accuracy is verified. The following conclusion can be drawn.

- A modification factor is introduced to modify the FRS

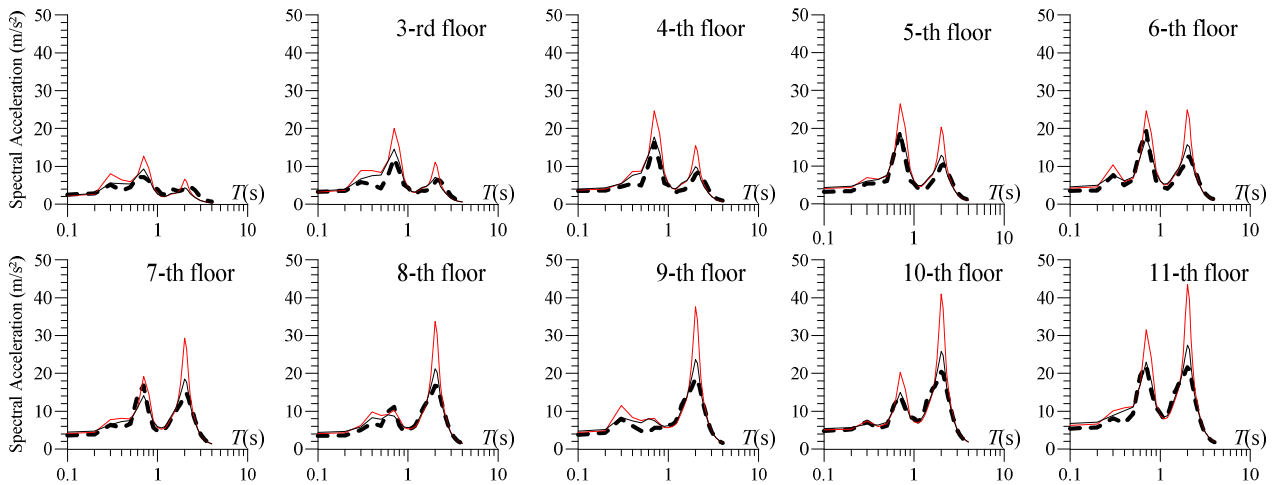


Fig. 17 Comparison of FRS derived from No. 18 ground motion in Table 4 (soil type D)

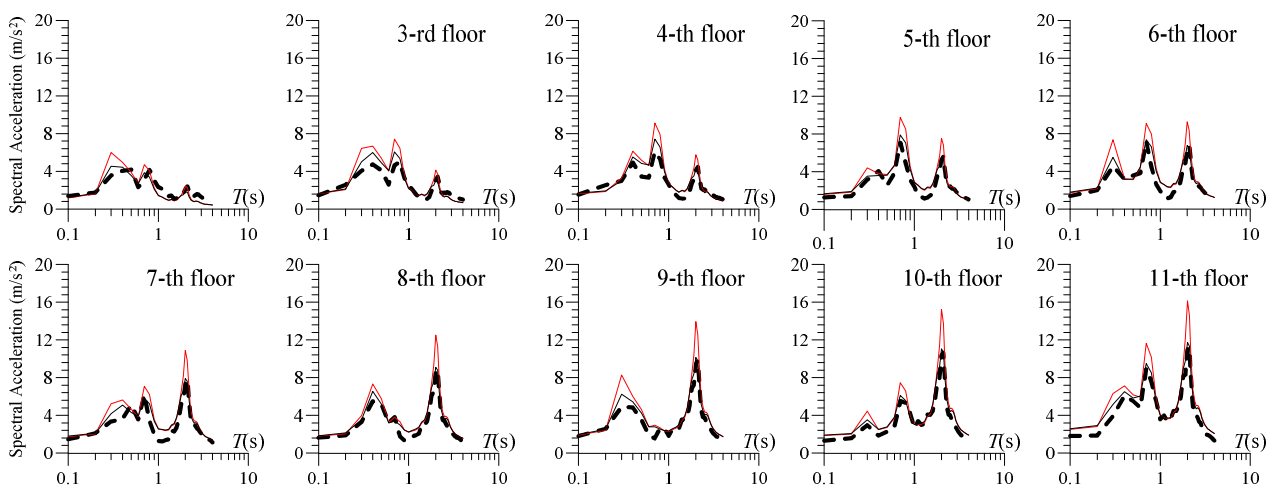


Fig. 18 Comparison of FRS derived from artificial ground motion

estimation method originally proposed by Yasui *et al.* (1993). The modification factor is defined as the ratio between the FRS estimated by the original method and the FRS computed by a time history analysis. A two-step procedure for deriving the modification factor is presented. The maximum values and the shape function of modification factors are estimated separately. Empirical functions of modification factors were built.

- The original method overestimates the FRS, and the effect of overestimation is more significant for real ground motions recorded on stiff sites, which has relatively short duration. Different modification factors were established for artificial and real ground motions.

- Because of the contribution of higher modes, the assumption of the damping model of the main structure may cause relatively large discrepancies in the FRS. With the dynamic properties of the nonstructural component in consideration, the damping model of the main structure should be carefully selected.

- The higher modes of the main structure may have a great effect on the FRS. The higher modes that can be neglected in the estimation of the response of the main structure may cause significant acceleration of the nonstructural component.

It should be noted that modification factors are derived under the conditions of assumed structural properties. Other factors such as the damping ratios of main structure and nonstructural component may also affect the modification factor. In case that different damping ratio is involved, specific analysis and validation is suggested.

References

- Baird, A., Tasligedik, A.S., Palermo, A. and Pampanin, S. (2014), "Seismic performance of vertical nonstructural components in the 22 February 2011 Christchurch earthquake", *Earthq. Spectra*, **30**(1), 401-425. <https://doi.org/10.1193/031013EQS067M>.
- Cai, C.Q. and Sheng, J.W. (1997), "Generating ground motion by two new techniques of adding harmonic wave in the time domain and approximation to response spectrum as a whole", *Acta Seismologica Sinica*, **19**(1), 87-96. <https://doi.org/10.1007/s11589-997-0043-x>.
- Flores, F.X., Lopez-Garcia, D. and Charney, F.A. (2015), "Assessment of floor accelerations in special steel moment frames", *J. Construct. Steel Res.*, **106**(106), 154-165. <https://doi.org/10.1016/j.jcsr.2014.12.006>.
- FEMA E-74 (2012), Reducing the Risks of Nonstructural Earthquake Damage – A Practical Guide, Federal Emergency

- Management Agency; Washington, D.C., USA.
- GB50011-2010 (2010), Code for Seismic Design of Buildings, National Standard of the People's Republic of China; Beijing, China.
- Ghosh, A.K. (2000), "Application of frequency domain analysis for generation of seismic floor response spectra", *Struct. Eng. Mech.*, **10**(1), 17-26. <https://doi.org/10.12989/sem.2000.10.1.017>.
- JSSI Manual (2003), *Design and Construction Manual for Passively Controlled Buildings*, Japan Society of Seismic Isolation (JSSI), First Edition; Tokyo, Japan.
- Kothari, P., Parulekar, Y.M., Reddy, G.R. and Gopalakrishnan N (2017), "In-structure response spectra considering nonlinearity of RCC structures: Experiments and analysis", *Nuclear Eng. Design*, **322**, 379-396. <https://doi.org/10.1016/j.nucengdes.2017.07.009>.
- Lihanand, K. and Tseng, W.S. (1988), "Development and application of realistic earthquake time histories compatible with multi-damping design spectra", *Proceedings of the 9th World Conference on Earthquake Engineering*, Tokyo, Japan, August.
- Mayes, R.L., Muraki, T., Jones, L.R. and Donikian, R. (1983), "Evaluation of methods used for the direct generation of response spectra", *Transactions of the 7th International Conference on Structural Mechanics in Reactor Technology (SMirt 7)*, Chicago, USA, August.
- Medina, R.A., Sankaranarayanan, R. and Kingston, K.M. (2006), "Floor response spectra for light components mounted on regular moment resisting frame structures", *Eng. Struct.*, **28**(14), 1927-1940. <https://doi.org/10.1016/j.engstruct.2006.03.022>.
- Miranda, E., Mosqueda, G., Retamales, R. and Pekcan, G. (2012), "Performance of nonstructural components during the 27 February 2010 Chile earthquake", *Earthq. Spectra*, **28**(S1), S453-S471. <https://doi.org/10.1193/1.4000032>.
- Oropeza, M., Favez, P. and Lestuzzi, P. (2010), "Seismic response of nonstructural components in case of nonlinear structures based on floor response spectra method", *Bullet. Earthq. Eng.*, **8**(2), 387-400. <https://doi.org/10.1007/s10518-009-9139-0>.
- Pan, X.L., Zheng, Z. and Wang, Z.Y. (2017), "Estimation of floor response spectra using modified modal pushover analysis", *Soil Dynam. Earthq. Eng.*, **92**, 472-487. <https://doi.org/10.1016/j.soildyn.2016.10.024>.
- Politopoulos, I. and Feau, C. (2007), "Some aspects of floor spectra of 1DOF nonlinear primary structures", *Earthq. Eng. Struct. Dynam.*, **36**, 975-993. <https://doi.org/10.1002/eqe.664>.
- Pozzi, M. and Der Kiureghian, A. (2015), "Response spectrum analysis for floor acceleration", *Earthq. Eng. Struct. Dynam.*, **44**(12), 2111-2127. <https://doi.org/10.1002/eqe.2583>.
- Saatcioglu, M., Tremblay, R., Mitchell, D., Ghobarah, A., Palermo, D., Simpson, R., Adebar, P., Ventura, C. and Hong, H. (2013), "Performance of steel buildings and nonstructural elements during the 27 February 2010 Maule (Chile) Earthquake", *Canadian J. Civil Eng.*, **40**(8), 722-734. <https://doi.org/10.1139/cjce-2012-0244>.
- Sankaranarayanan, R. and Medina, R.A. (2007), "Acceleration response modification factors for nonstructural components attached to inelastic moment-resisting frame structures", *Earthq. Eng. Struct. Dynam.*, **36**, 2189-2210. <https://doi.org/10.1002/eqe.724>.
- Seismosoft (2013), *SeismoArtif v2.1.0 – A New Tool for Artificial Accelerograms Generation*; Seismosoft, Pavia, Italy. <http://www.seismosoft.com>.
- Shooshtari, M., Saatcioglu, M., Naumoski, N. and Foo, S. (2010), "Floor response spectra for seismic design of operational and functional components of concrete buildings in Canada", *Canadian J. Civil Eng.*, **37**(12), 1590-1599. <https://doi.org/10.1139/L10-094>.
- Singh, M.P. and Chang, T.S. (1996), "Floor response spectrum amplification due to yielding of supporting structures", *Eleventh World Conference on Earthquake Engineering*, Acapulco, Mexico, June.
- Vukobratovic, V. and Fajfar, P. (2015), "A method for the direct determination of approximate floor response spectra for SDOF inelastic structures", *Bullet. Earthq. Eng.*, **13**(5), 1405-1424. <https://doi.org/10.1007/s10518-014-9667-0>.
- Vukobratovic, V. and Fajfar, P. (2016), "A method for the direct estimation of floor acceleration spectra for elastic and inelastic MDOF structures", *Bullet. Earthq. Eng.*, **45**(15), 2495-2511. <https://doi.org/10.1002/eqe.2779>.
- Yasui, Y., Yoshihara, J., Takeda, T. and Miyamoto, A. (1993), "Direct generation method for floor response spectra", *Transactions of the 12th International Conference on Structural Mechanics in Reactor Technology (SMIRT 12)*, Stuttgart, Germany, August.

CC